Impact of Mixed Convection on the Cooling Kinetics of Heat-Generating Products Within a Ventilated Pallet: Application to Cheese

Dihia Aguenihanai, Denis Flick, Steven Duret, Elyamin Dahmana, Jean Moureh

Impact of mixed convection on the cooling kinetics of heat-generating products within a ventilated pallet: Application to cheese

Dihia AGUENIHANAI*[(a,b)], Denis FLICK[(c)], Steven DURET[(a)], Elyamin DAHMANA[(a)], Jean MOUREH[(a)]

[(a)] Université Paris-Saclay, INRAE, FRISE, 92761, Antony, France

[(b)] CNIEL, 75009, Paris, France

[(c)] Université Paris-Saclay, AgroParisTech, INRAE, UMR SayFood, 91120, Palaiseau, France

*Corresponding author: dihia.aguenihanai@inrae.fr

Abstract

Cheese temperature control in the cold chain is essential for quality preservation and waste reduction, especially for soft cheeses, which generate heat due to their microbiological activity. This study first analyses, at steady state, the natural convection effect on the temperature distribution along three pallet rows (from upstream to downstream). Second, it investigates, under unsteady state, the effect of upwind air velocity (0.25 m/s and 0.64 m/s), product heat generation (0 W, 0.05 W, and 0.3 W per product item), and initial product temperature heterogeneity on the cooling rate within a ventilated pallet in a cold room. The cheeses were replaced with plaster cylinders equipped with controllable resistance heaters to simulate heat generation by cheeses. At steady state, the temperature measurements confirmed the presence of a thermal plume on the pallet downstream row when natural convection was predominant (Richardson number = 6.53). Under unsteady state conditions, increasing the air velocity from 0.25 m/s to 0.64 m/s reduced the Half Cooling Time (HCT) and Seven-Eighths Cooling Time (SECT) by at least 26% and 37%, respectively. Greater heat generation increased the product temperature but, interestingly, reduced the product cooling time.

Keywords: Soft cheese, heat-generating product, ventilated pallet, cooling kinetics, thermal plume, mixed convection.

Nomenclature

$\dot{m}$	Airflow rate, kg/s
a	Cooling coefficient ($a = 1/\tau = h\ S/(m\ Cp)$), s^{-1}
b	$b = \frac{n\ h\ S}{\dot{m}\ Cp_{air}}$, [-]
C_p	Heat capacity at constant pressure, J/(kg K)
D	Cheese diameter, m
h	Convective heat transfer coefficient, W/(m^2 K)
k	Coverage factor
m	Product mass, kg
n	Cheese products number, n = 30 in one box of product
Q	Heat generation flux per product item (250 g of cheese), W
$Q_{heat.tot}$	Heat generation flux per box of product ($Q_{heat.tot}$ = 30Q), W
S	Product exchange surface, m^2
t	Time, s
T	Temperature, °C
T^*	Dimensionless temperature, [-]
u	Air velocity, m/s
u_{exp}	Experimental standard uncertainty
U_{exp}	Experimental expanded uncertainty
β_T	Thermal expansion coefficient, K^{-1}
Dimensionless numbers	
Bi	Biot number, [-]
Gr	Grashof number, [-]
Pr	Prandtl number, [-]
Ra	Rayleigh number, [-]
Re	Reynolds number, [-]
Ri	Richardson number, [-]
Greek symbols	
μ	Dynamic viscosity, kg/(m s)
ν	Kinematic viscosity, m^2/s
ρ	Density, kg/m^3
λ	Thermal conductivity, W/(m K)
δ	Adiabatic heating rate ($\delta = Q/(m\ Cp)$), °C/s
Abbreviations	
BB	Big block: equivalent to 15 cheese product items
CHTC	Convective Heat Transfer Coefficient, W/(m^2 K)
HCT	Half Cooling Time, hours
SB	Small block: equivalent to one cheese product item
SECT	Seven-Eighths Cooling Time, hours

STD	Standard Deviation
Subscripts	
air	Airflow
air.in	Upwind airflow
eq	Equilibrium / Final
Exp	Experimental
Het	Heterogeneous
Hom	Homogeneous
in	Initial
Max	Maximum
Num	Numerical
p	Product

1. Introduction

To preserve the taste quality of the cheese and to reduce product waste, it is essential to cool products quickly and uniformly following production and the palletization processes. Maintaining the cheese temperature below the appropriate value during the supply chain remains challenging, particularly for soft cheeses. Indeed, soft cheeses are microbiologically active and generate a large amount of heat (Pham et al. 2019a).

The efficiency and the cooling rates of the products depend on several parameters linked mainly to ventilation conditions (e.g. airflow rate (Han et al. 2015), product position; (Wu et al. 2019)), packaging design (e.g. total area of openings (Agyeman et al. 2023), shape (Ambaw et al. 2017), the positions of vents (O’Sullivan et al. 2017), polylined products (Ambaw et al. 2017)), pallet arrangement (Sajadiye and Zolfaghari 2017), and physiological mechanisms such as heat generation and the initial product temperature prior to storage (Berry et al. 2021). Among those parameters, the airflow velocity around the products is one of the most significant, as it is linked directly to the convective heat transfer coefficient (CHTC) (Alvarez and Flick 1999). For example, According to Wang et al. (2020), increasing the airflow velocity by 500% halved the seven-eighths cooling time (SECT) of apple products within a box.

To improve cooling efficiency and ensure rapid and uniform cooling, many studies have investigated the impact of packaging design on airflow and heat transfer within ventilated packages, for instance (Agyeman et al. 2023) for tomatoes, (Ambaw et al. 2017) for pomegranates, and (Berry et al. 2021) for citrus fruit. The effect of the total area of the openings is often studied since increasing the total area of the openings in the packaging reduces the temperature heterogeneity and pressure loss. Nevertheless, it slightly affects the SECT of the products: for a constant air velocity, the SECT decreases by 14% when the area of the openings is increased from 9.1% to 64.4% (Wang et al. 2020). Therefore, the vents' position and connection are particularly important when the products are stacked in several layers within the boxes, as considerable cooling heterogeneity and loss of quality can occur within the same box (Han et al. 2018).

Beyond the initial temperature conditions and the design factors, the heat generation of cheese products exerts an impact on their temperature heterogeneity (Aguenihanai et al. 2025; Pham et al. 2021). An increase in the heat-generated flux increases the temperature of the products and thus the natural convection, while forced airflow becomes weaker downstream from the pallet as air passes through the lateral vents of the boxes (Pham et al. 2021). Hence, natural and forced convection may be of the same order of magnitude, resulting in mixed convection that needs to be considered (Joye 2003). To characterize whether the convection is free, forced or mixed, the Richardson dimensionless number (Ri) is calculated. The Richardson number is expressed using the Grashof number (natural convection) and the Reynolds number (forced convection) ($Ri = Gr/Re^2$). Natural convection is negligible for Ri << 1, forced convection is negligible for Ri >> 1, while mixed convection should be considered for Ri ≅ 1 (Ozisik 1985). In stacked food products, at low air velocities (<0.1 m/s), heat transfer may no longer be governed by forced convection (Le Page et al. 2009). Regarding the impact of free convection on heat transfer, mixed convection can be divided into three cases (Dawood et al. 2015): 1- the buoyant motion and the forced motion are in the same direction, which enhances heat transfer; 2- natural convection opposes forced convection, which may result in either diminished or enhanced heat transfer; 3- the buoyant motion acts perpendicular to the forced motion, which improves fluid mixing and heat transfer.

Therefore, in the case of heat-generating products such as cheeses within a ventilated pallet, the interaction between free and forced convection needs to be considered in order to optimize product temperature control. However, while numerous studies have been carried out in order to characterize the thermal heterogeneity within one level of a pallet along the main flow direction (from the ventilated face to the opposite one) under a forced convection regime such as (Ambaw et al. 2013) and (Han et al. 2018), limited research has focused on the cooling rate of heat-generating products stacked within ventilated pallets under mixed convection. To the best of the authors' knowledge, only Chourasia and Goswami (2007a) have studied the impact of heat generation on the cooling time of a single stack of potatoes in a storage room, and these authors confirmed that the heat generation of the products affects the cooling process. In this study, Chourasia and Goswami (2007a) neglected the interaction effect between different stacks and numerically predicted the effect of natural convection on the internal airflow without experimental validation. No experimental work that characterizes the thermal heterogeneity along the pallet height has been carried out within a pallet of heat-generating products. The resulting vertical thermal gradient through the ventilated pallet reflects dynamic interactions between the horizontal forced convection flow induced by fans and the vertical flow generated by natural convection through the bottom vents of the cardboard box.

This study aimed to investigate the combined effect of airflow, heat generation of the soft cheeses and the homogeneous or heterogeneous initial temperature on the cooling rate of the products within an entire pallet comprising nine levels of ventilated boxes with vents on the lateral and bottom sides. The thermal heterogeneity was investigated in the horizontal direction through the main flow and also in the vertical direction through the nine levels composing the pallet. This study provides an in-depth insight into the cooling process of heat-generating products and their different cooling trends under steady and unsteady state conditions. It quantitatively analyses the HCT and SECT of products under different convection conditions for different Richardson numbers, 0, 0.17, 1.09 and 6.53, reflecting predominant forced convection and predominant mixed convection and natural convection, respectively. A simple model has been developed to interpret the experimental results.

2. Materials and methods

2.1 Experimental device

The experimental device consisted of an industrial-sized cheese pallet (800 mm × 1200 mm × 1455 mm) comprising nine levels positioned inside a cold room with controlled upwind air velocity and temperature (see Fig. 1). Each level was subdivided into six boxes separated by 1-cm gaps. The boxes' sides and bottom were vented (Fig. 1(c, d, e)). Each box contained 30 cheese products arranged in three layers (see Fig. 2).

The cheeses were replaced with two types of plaster blocks: small blocks (SBs) and big blocks (BBs), as illustrated in Fig. 2. The small blocks (SBs) are designed to replicate the dimensions of industrial cheese products (D = 110 mm and H = 40 mm) and were placed at the 8^{th} level (k = 8). Each box at this level contained 30 small blocks. The big block (BB) is equivalent to fifteen product items. From the 1^{st} to the 7^{th} and 9^{th} levels, boxes contain BBs. Each box at these levels contained two BBs.

All the plaster blocks were equipped with controllable resistance heaters to accurately simulate the heat generation of the products (Q per cheese item of 250 g); for additional details, see (Pham et al. 2019a). An electrical generator supplied the controllable resistance heaters with a voltage measurement accuracy of 0.05% + 15 mV and a current measurement accuracy of 0.1% + 60 mA (manufacturer's data). Heat output (in watts) was controlled by varying the voltage of the electrical generator. The expanded uncertainty of the heat output, with a coverage factor k = 2, is ± 0.001 W for 0.05 W (representing 0.3% of the set value) and ± 0.003 W for 0.3 W (1% of the set value).

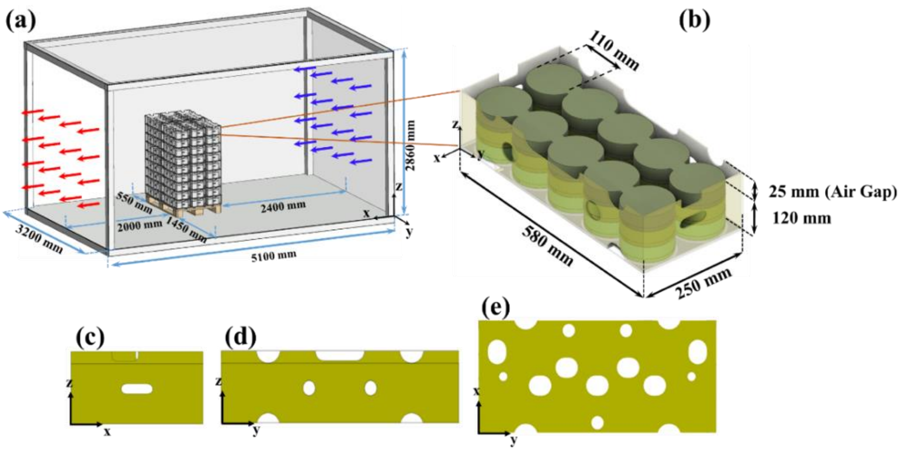

Fig. 1. Diagram showing the experimental device: (a) pallet within a cold room; (b) 3D view of one box containing 30 cheese items; (c) lateral view of the box; (d) frontal view of the box; (e) bottom view of the box.

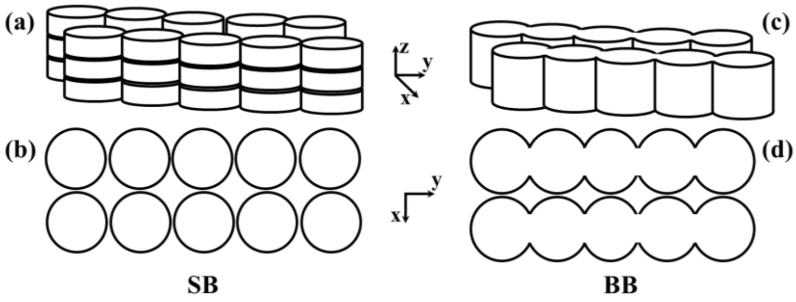

Fig. 2. Diagram showing the different types of plaster blocks: (a) lateral view of the small blocks; (b) view of the small blocks from above; (c) lateral view of the big blocks; (d) view of the big blocks from above.

2.2 Temperature measurements

In this study, temperature measurements were obtained using T-type thermocouples with an experimental standard uncertainty u_{exp} of ± 0.2°C (including thermocouple calibration, bath calibration and repetition uncertainties). The expanded uncertainty U_{exp} for a coverage factor (k = 2) is ± 0.4°C. These thermocouples were individually calibrated between 0 and 40°C. Data acquisition was carried out on half of the experimental set-up (Fig. 3).

It is important to note that only the BBs were instrumented for temperature monitoring (from k = 1 to 7 and k = 9). In each box (B_1, B_2 and B_3) at these levels, one of the central products of the BB was instrumented at the mid-height. Three rows within the pallet were thus instrumented from upstream to downstream (Row R_1, Row R_2 and Row R_3) (see Fig. 3). Furthermore, as illustrated in Fig. 3b, at level 8 (k = 8), three additional thermocouples were added in the air gap between each of the B_1, B_2 and B_3 boxes in order to perform air temperature measurements. Temperature measurements were recorded once every minute using BenchLink Data Logger software.

At steady state, three repetitions were carried out for two cooling experiments at an air temperature of 4°C: $u_{air.in}$ = 0.25 m/s & Q = 0.3 W and $u_{air.in}$ = 0.64 m/s & Q = 0.05 W. The maximum standard deviation obtained at steady state was 0.3°C.

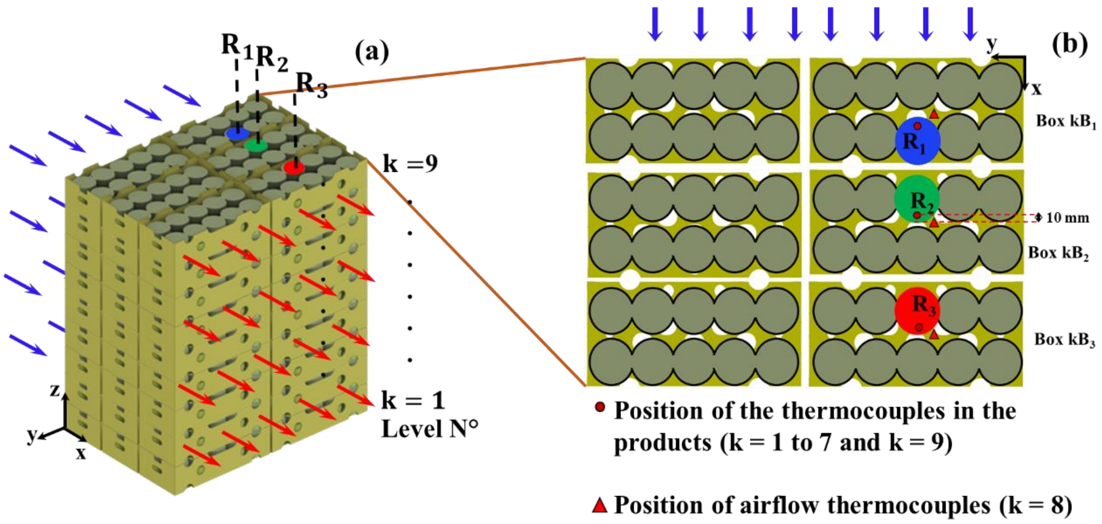

Fig. 3. Illustration of (a) the position of rows R_1, R_2 and R_3; (b) the instrumented plaster product positions (k = 1 to 7 and k = 9) and airflow thermocouple positions (k = 8).

2.3 Experimental process

2.3.1 Experimental stages

Initialisation stage:

This study investigated two initial product temperature conditions: homogeneous and heterogeneous initial temperatures. According to the heat balance for heat-generating products at steady state:

$$m\, C_p\, \frac{dT}{dt} = h\, S\, (T_{air} - \mathrm{T}) + Q \quad \text{with } \frac{dT}{dt} = 0$$

- Homogeneous initial temperature ($T = T_{air} = T_{air.in}$)

The controllable resistance heaters were turned off (Q = 0 W), and the air temperature was set to 20°C. Once thermal equilibrium was achieved, the pallet was at a homogeneous initial temperature with $T = T_{air.in}$ (≈ 20°C). For homogeneous initial conditions, the standard deviation of the temperature in the entire pallet at the beginning of cooling was 0.2°C. This scenario reproduces the thermal state of the pallet just after the production stage prior to pre-cooling.

- Heterogeneous initial temperature ($T = T_{air} + Q/(hS)$)

The temperature of the upwind air was set at 20°C with the resistance heaters turned on until a thermal equilibrium had been achieved. Thus, the products within the pallet were at different initial temperatures ($T = T_{air} + Q/(hS)$). This experiment aimed to reproduce cases where the products have generated heat, achieved a thermal equilibrium, and then have undergone ambient temperature changes, for example, when pallets are transferred between two facilities within a logistic cold chain.

Insulation stage:

As previously mentioned, the initial upwind air temperature was set at 20°C. To begin the cooling process of products within the pallet, the upwind air temperature was set at 4°C. However, the temperature decrease was gradual, reaching 4°C in about an hour.

During this stage, it is important to maintain the initial temperature defined in the initialization stage (see the section above), in order to estimate the cooling rate of the products accurately. Thus, the pallet was insulated using extruded polystyrene insulation panels wrapped in isothermal survival blankets for additional thermal protection. Although the panels were not completely airtight, the average temperature of the products in box $9B_1$ (see Fig. 3) decreased by ≈ 1°C during the insulation phase, whereas it decreased by ≈ 8°C without the panels.

It is important to note that in the case of a heterogeneous initial temperature of the pallet, the resistance heater of the products is deactivated during this stage and then reactivated once the insulation phase is completed. In the case of a homogeneous initial temperature, the resistance heater is activated following the insulation stage.

Cooling stage:

Once the two previous steps have been completed and the insulation panels have been removed, the cooling process to a set-point temperature of 4°C is considered to have started.

2.3.2 Experimental conditions and thermophysical properties

According to a calorimetric study carried out in our laboratory on Camembert-type soft cheeses, the heat flux Q generated by one product item (250 g) is estimated to be between 0.1 W and 0.15 W (Confidential report (Delahaye et al. 2019)). In fact, the respiration heat depends on the temperature and the ripening stage. Under industrial conditions during transport and storage, the air velocity can vary from 0.1 to 1 m/s, depending on the position of the pallets (Hoang et al. 2015; Moureh et al. 2009). The balance between heat generation, which contributes to free convection, and ventilation can be analysed in terms of Richardson number, Ri; therefore, increasing heat generation is equivalent to reducing ventilation. Under these conditions (Q = 0.1 W, velocity between 0.1 and 1 $m.s^{-1}$), Ri is between 0.14 and 13.6.

In this study, two upwind air velocities $u_{air.in}$: 0.25 m/s and 0.64 m/s (chosen according to cold room ventilation capacities ranged between 0.25m/s and 0.64 m/s), and three heat generation fluxes per product item, Q: 0 W, 0.05 W and 0.3 W were investigated. Table 1 summarises the dimensionless numbers under each condition. The diameter of one SB plaster block was chosen as the characteristic length. It can be observed that the range of variation of Ri (0.17 to 6.53) is comparable to that observed under industrial conditions.

Table 1: Dimensionless numbers of each experimental condition

$u_{air.in}$ (m/s)	Re (-)	Q(W)	Ri (-)
0.25	1752	0	0
		0.05	1.09
		0.3	6.53
0.64	4484	0	0
		0.05	0.17
		0.3	1

$$\mathrm{Re} = \frac{u_{air.in} D}{\nu} \tag{1}$$

$$\mathrm{Gr} = \frac{g\beta_T Q D^2}{\lambda_{air}\, \nu^2} \tag{2}$$

$$\mathrm{Ri} = \frac{\mathrm{Gr}}{\mathrm{Re}^2} = \frac{g\beta_T Q}{\lambda_{air}\, u_{air.in}^2} \tag{3}$$

where: D = 0.11 m; $\nu = 15.7\times10^{-6}$ m^2/s; $\lambda_{air} = 0.026$ W/(m K); $\beta_T = 1/T_{air.in} = 0.0036$ K^{-1}.

According to Bejan (2013), the critical Reynolds number obtained using round jets such as circular vents is about 30. Thus, from Table 1, the flow was considered turbulent. The airflow was under a mixed convection regime when Ri ≈ 1. The airflow is dominated by forced convection at low Richardson number (Ri << 1) and by natural convection at high Richardson number (Ri >>1) (Pham et al. 2019b; Tanner et al. 2002). This also gives a range of Ri from 0.17 (relatively small compared to 1), where forced convection should dominate, to 6.53 (relatively large compard to 1) where free convection should dominate.

The thermal conductivities of plaster and cheese are close: 0.35 $W.m^{-1}K^{-1}$ for plaster and between 0.32 and 0.38 $W.m^{-1}K^{-1}$ for cheese, depending on the type of cheese (Iezzi et al. 2011). Thus, cheese and plaster exhibit similar temperature levels at steady state. However, the density and heat capacity are different: $\rho.C_p$ of about 1.4×10^6 $J.m^{-3}K^{-1}$ for plaster and 2.3×10^6 $J.m^{-3}K^{-1}$ for cheese (Božiková and Hlaváč 2016; Hélias et al. 2007). Therefore, cheese and plaster exhibit different cooling kinetics at unsteady state, where for equal conductivity and no heat generation, characteristic cooling times (HCT and SECT) for cheese products are expected to be around 1.6 ($(\rho\ C_p)_{Cheese}/(\rho\ C_p)_{Plaster}$) times higher than for plaster blocks.

It is important to mention that a CFD model will be developed as a further step. The properties of plaster will be applied initially to reproduce the experimental conditions and validate the model in comparison with the experimental results presented in this study. Once the model has been validated, the thermophysical properties of cheese will be applied to predict the cooling kinetics of cheese products within a pallet.

The thermophysical properties of the materials used in the experiment are shown in Table 2.

Table 2: Thermophysical properties of the experimental materials

Materials	ρ (kg/m³)	λ (W/(m K))	c_p(J/(kg K))
Plaster (Pham et al. 2019b; Ruuska et al. 2017)	1240	0.35	1100
Air	1.269	0.026	1006

2.4 Cooling rate evaluation

Because of heat generation, the plaster product equilibrium temperature at the end of the cooling process is different from the temperature of upwind air (Pham et al. 2021). In addition, the initial product temperature differs from one product to another under the initial heterogeneous temperature conditions.

To quantify the cooling rate of the products within the pallet and compare the different experimental conditions, a new dimensionless temperature definition was established:

$$T^{*}(t) = \frac{T(t) - T_{eq}}{T_{in} - T_{eq}} \quad (4)$$

where:

T_{in} is the initial temperature of the product at the beginning of the cooling stage ($T_{in} = T(t=0)$).

T_{eq} is the equilibrium temperature of the product. It is calculated using the average of the temperature values of the last 30 minutes once the equilibrium temperature is achieved.

The equilibrium temperature is considered to have been reached when the average product temperature decreases less than 0.02°C per 30 minutes.

Studies reported in the literature often use two parameters to assess the product cooling rate: the seven-eighths cooling time (SECT) and the half cooling time (HCT). SECT represents the time required to reduce the difference between the initial temperature of the product T_{in} and its equilibrium temperature by 87.5% (T^{*}(SECT) = 0.125). Meanwhile, the HCT represents the time needed to reduce this temperature difference by 50% (T^{*}(HCT) = 0.5) (Defraeye et al. 2014).

2.5 Statistical analysis

Statistical analysis One-way variance analysis (ANOVA), followed by a Tukey's HSD test, were conducted to assess the significance of T_{in}, T_{eq}, HCT and SECT along the different rows of the pallet. This analysis allows to evaluate if the effect of different tested conditions (inlet air velocity, heat generation, initial temperature condition) on HCT and SECT is statistically significant with a critical p-value of 5% ($p \leq 0.05$).

2.6 Interpretation of the results using a simple model

A very simple model was developed, not for accurate prediction but to facilitate the interpretation of the experimental data. As shown in Fig. 4a, this unsteady state model considers the air temperature increase when it flows throughout the three boxes successively. It considers a half level of the pallet. The heat generated by the plaster products in each box ($Q_{heat.tot} = n\,Q$, where n = 30) is considered.

The model is based on the following assumptions:

- Symmetry at one pallet level is considered. Only half of the pallet level is taken into account by the model.
- The interaction between the different levels of the pallet is neglected.
- The model considers the product heat generation but not the promoted natural convection.
- The CHTC is considered a constant (independent of airflow velocity and block positions).
- The airflow rate within the boxes is considered a constant.

- $T_{air.in}$ is considered equal to the set-point value, which is 4°C.
- The initial product temperature equals the initial experimental product temperature after the insulation stage (≈ 19°C).
- T_i for $i \in [1, 3]$ represents the average product temperature of each box.
- $T_{air.i}$ for $i \in [1, 3]$ is the bulk air temperature at the outlet of box i.

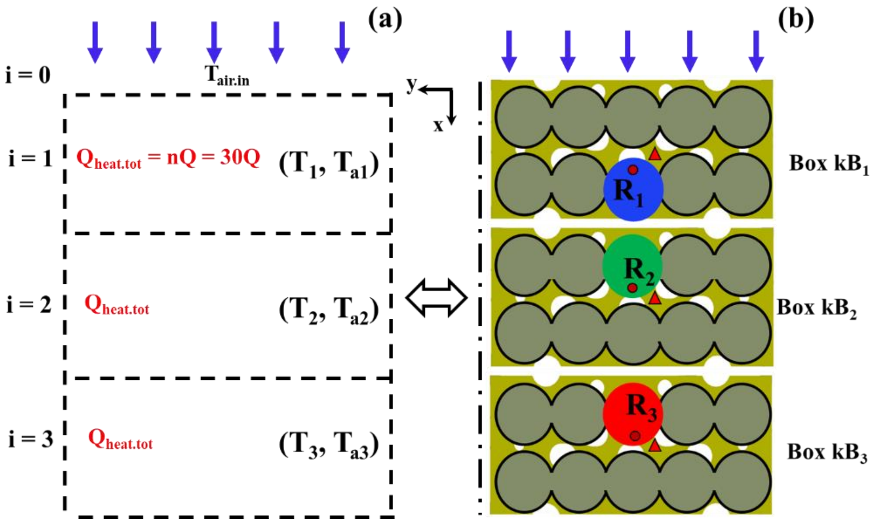

Fig. 4. Diagram of the domain: (a) simplified heat transfer domain; (b) representation of the top view of the experimental set-up.

The heat balance for the product and air can be expressed as follows:

$$m\,C_p\,\frac{dT_i}{dt} = h\,S\,(T_{air.i-1} - T_i) + Q \quad \text{for } i \in [1,3] \tag{5}$$

$$\Leftrightarrow \frac{dT_i}{dt} = a\,(T_{air.i-1} - T_i) + \delta \tag{6}$$

$$\dot{m}\,C_{p.air}\,(T_{air.i} - T_{air.i-1}) = n\,h\,S\,(T_i - T_{air.i-1}) \quad \text{for } i \in [1,3] \tag{7}$$

$$\Leftrightarrow T_{air.i} = T_{air.i-1} + b\,(T_i - T_{air.i-1}) \tag{8}$$

where: $a = \frac{h\,S}{m\,C_p}$, $\delta = \frac{Q}{m\,C_p}$ and $b = \frac{n\,h\,S}{\dot{m}\,C_{p.air}}$

The adiabatic heating rate, that is, the product temperature increase per time unit without heat exchange with air: δ equals 0.45°C/h and 2.68°C/h for Q = 0.05W and Q = 0.3 W, respectively. The optimum values for a and b have been determined by adjustment with the experimental data.

3. Results and discussion

3.1 Steady state

Fig. 5 compares the measured temperature distribution obtained at steady state through the rows R_1, R_2 and R_3 for two upwind air velocities (0.25 m/s and 0.64 m/s) and two heat generation fluxes per product item (0.3 W and 0.05 W). Thus, this section presents the results of four different Richardson numbers.

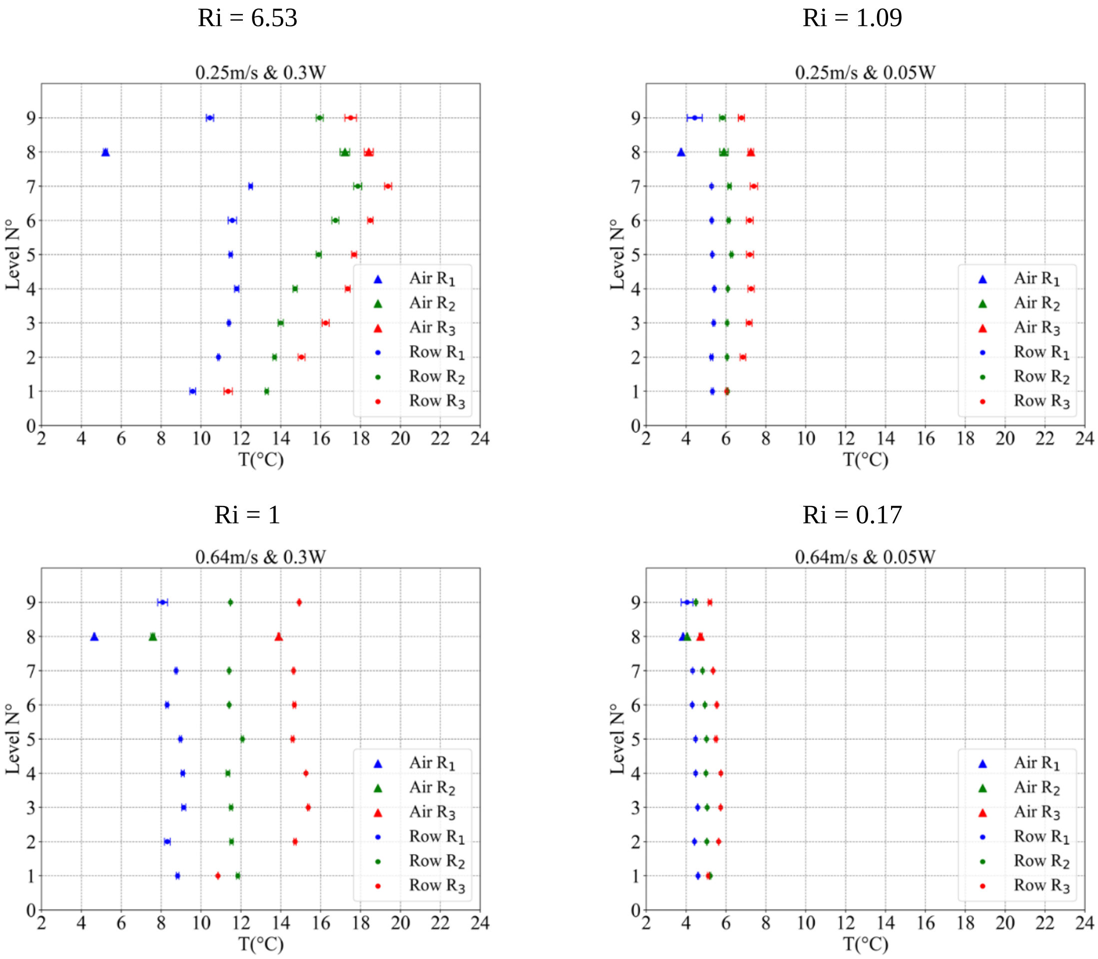

Fig. 5. Plaster product temperature distribution at steady state along the Rows R_1, R_2 and R_3 and air temperature (Level 8) for two upwind air velocities, 0.25 m/s and 0.64 m/s, and two heat-generated fluxes per product item, 0.05 W and 0.3 W. Note: standard deviation bars are added to each temperature point.

According to Fig. 5, for both upwind air velocities conditions, at each level (from k = 2 to 9 (top of the pallet), with the exception of the bottom of the pallet (k = 1), which is explained later), the product temperature increases from upstream to downstream of the pallet ($T(R_1) < T(R_2) < T(R_3)$). This temperature increase is induced by the rising air temperature in the main airflow direction in contact with the products ($T_{air}(R_1) < T_{air}(R_2) < T_{air}(R_3)$) and by the decrease in airflow rate in the main flow direction caused by the exit of part of the flow through the side vents of the boxes and the spaces between them (Aguenihanai et al. 2025), thus reducing the convective heat transfer coefficients (Pham et al. 2021). Furthermore, the heat flux generated by the product significantly impacts the product temperature and its heterogeneity within a pallet. The greater the heat flux, the higher the product temperature and the temperature heterogeneity. These results are consistent with the literature (Pham et al. 2021).

For lower Ri (Ri ≤ 1), where the dominant convection mechanism is forced convection (0.25 m/s and 0.05 W, 0.64 m/s and 0.05 W, and 0.64 m/s and 0.3 W), a quasi-homogenous product temperature distribution per row can be observed. For example, in the case of 0.64 m/s & 0.3 W (Ri = 1), the difference between the maximum and minimum measured temperatures is less than 1°C for rows R_1 and R_2. However, it is higher in the downstream part of the pallet (row R_3), reaching 4.5°C.

For higher Ri (Ri > 1), the quasi-linear increase in the product temperature in R_3 and R_2 (from k = 2 to k = 7) reflects the emergence of a vertical flow within the pallet through the ventilated boxes under a mixed convection regime. The driving force of this vertical flow induced by natural convection is enhanced by the temperature difference between the warm, heat-generating products and the ambient cold air, and thus, it is likely to predominate in the downstream part of the pallet at rows R_2 and R_3 (Fig. 5).

As mentioned in Section 2.1, the bottom of the boxes includes vents allowing inter-level interaction (upward flow) and aiming to promote internal ventilation within the pallet. This warmed air rises by buoyancy resembling a thermal plume into the upper-level box through the free vents at the bottom of the boxes. This phenomenon is associated with the ejection mechanism (Khanafer et al. 2002). Therefore, cold air is sucked in from the bottom of the pallet and from the sides to replace the hot air moving towards the upper level (Chourasia and Goswami 2006, 2007). This enables product heat to be removed from one level to the next in the vertical direction, leading to a product temperature increase in the horizontal direction in the main flow direction (from R_1 to R_3) and also in the vertical direction by the effect of the upward flow (the vertical temperature increase reaches 8.2°C in row R_3).

The measured temperature increases in the vertical direction of the pallet until the penultimate level. The temperature decreases at the top of the pallet (k = 9) due to direct contact between the products and the cold ambient air.

At the bottom level of the pallet (k = 1), boxes in B_3 located in the more downstream position are subjected to warmer airflow through B_1 and B_2, leading to greater buoyancy and vertical flow. This raises air suction at the first level of B_3 (Box $1B_3$), leading to a lower temperature in Box $1B_3$ compared to that in Box $1B_2$. Obviously, this additional ventilation induced by natural convection is limited to the first level of the pallet for moderate and low Ri values (equal to or less than one), given that a quasi-homogenous temperature for the rows R_3, R_2 and R_1 is observed at the other levels.

For our complex geometry, we can conclude that for Ri = 0.17, the regime is dominated by forced convection; for Ri ≈ 1, the effect of natural convection becomes visible and for Ri = 6.53 its effect is very pronounced. However, it is difficult to determine a precise value of Ri for which forced and free convection are of the same order. As expected, the greater Ri, the greater the intensity of the thermal plume (vertical flow due to the temperature gradient), particularly downstream of the pallet. Thus, an increase in the vertical flow intensity is associated with a more significant suction of surrounding cold air at 4°C. As was observed at box $1B_3$ in the case of Ri = 6.53, with a temperature $T(1B_3) < T(1B_2)$. This phenomenon (under high Ri number) allows heat to be rapidly extracted from the products and cooled more quickly than under low Richardson numbers (see section 3.2.2 Heat generation effect).

These results demonstrate the importance of designing vents at the bottom of the boxes to ensure free ventilation by natural convection and thus to enhance removal of the heat generated by the products. It is also important to ensure that the stacking of the products in the boxes does not obstruct, or obstructs to the least extent possible, these vents. In this manner, they prevent heat from stagnating inside the boxes and avoid the generation of higher product temperatures.

A previous study (Pham et al. 2019a, 2019b) also pointed out the importance of the area of the openings (vent holes) in the ventilation direction related to the upstream velocity. Cheese stacking should not obstruct these vents, and it is important to position the pallet on the side with the highest total area of openings in order to increase the flow rate through the boxes, thereby increasing the convective heat transfer coefficient (CHTC) and decreasing the temperature levels.

3.2 Unsteady state

3.2.1 Ventilation velocity effect

The products' dimensional and dimensionless cooling kinetics are presented in Fig. 6 for two upwind air velocities (0.25 m/s and 0.64 m/s) without heat generation (Q = 0, Ri = 0). The corresponding SECT and HCT of each row R_1, R_2 and R_3 are presented in Table 3 for each air velocity condition.

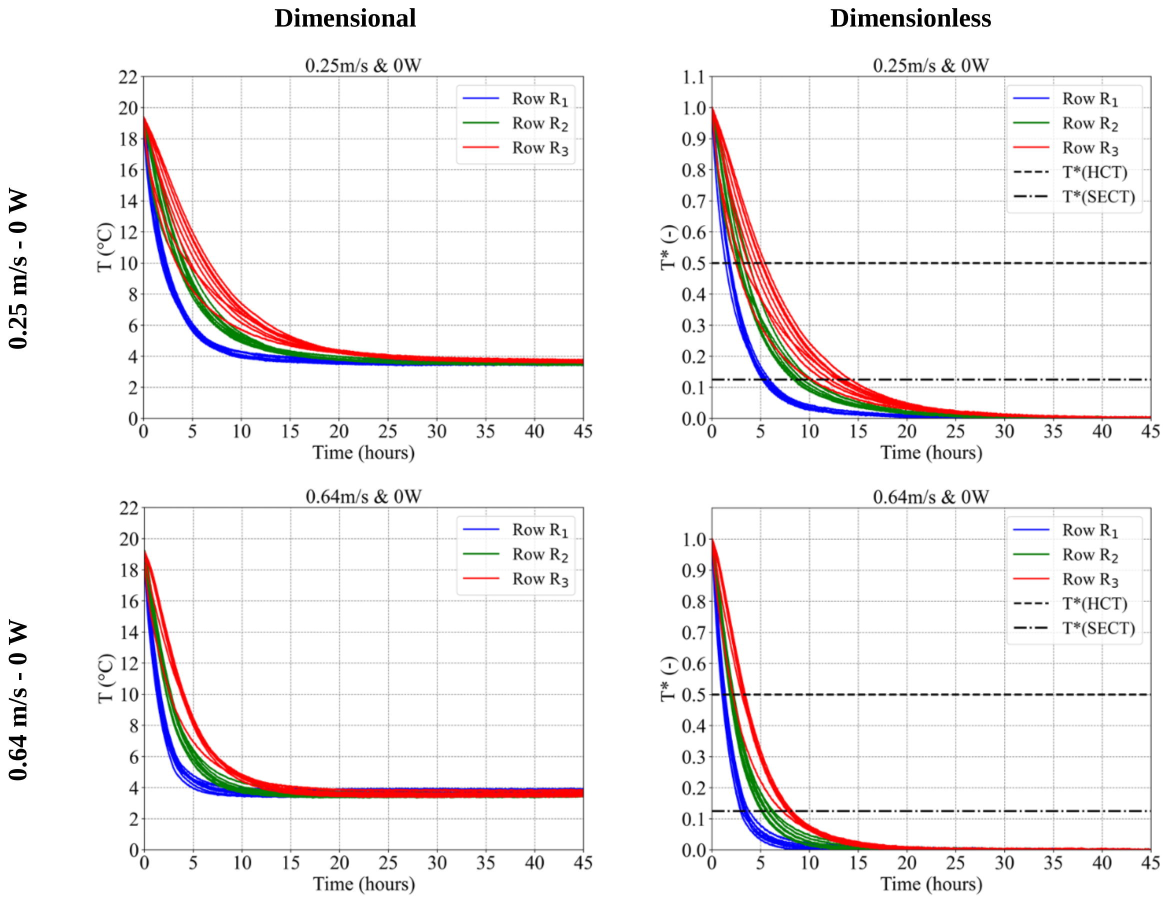

Fig. 6. Dimensional and dimensionless cooling kinetics of the plaster products within the pallet along the rows R_1, R_2 and R_3 for two upwind air velocities: 0.25 m/s and 0.64 m/s and 0 W.

Table 3: Summary of the average HCT, SECT and their standard deviation within the different pallet rows (R_1, R_2 and R_3) for the two velocities, 0.25 m/s and 0.64 m/s, and a product flux equal to 0 W. Different letters (e.g., 'a', 'b') indicate significant differences ($p < 0.05$) based on Tukey HSD test.

Upwind air velocity $u_{air.in}$ (m/s)	**0.25**			**0.64**		
Heat generation flux Q (W)	**0**			**0**		
Row	**R_1**	**R_2**	**R_3**	**R_1**	**R_2**	**R_3**
HCT ± STD_{HCT} per row (hours)	**1.71** ± $0.15^{a,b}$	**3.06** ± 0.41^{c}	**4.21** ± 0.97^{d}	**1.25** ± 0.11^{a}	**2.06** ± 0.13^{b}	**3.10** ± 0.37^{c}
SECT ± STD_{SECT} per row (hours)	**5.50** ± 0.21^{a}	**9.21** ± 0.68^{b}	**12.58**±1.23^{c}	**3.41** ± 0.26^{d}	**5.68** ± 0.32^{a}	**7.93** ± 0.29^{e}

For all conditions presented in Fig. 7, the products near the air inlet (R_1) cooled down more rapidly than the other products (R_2 and R_3, $p \leq 0.05$). According to Table 3, increasing the air inlet velocity from 0.25 m/s to 0.64 m/s reduces the SECT and HCT of the products along the different rows by an average of 38%. These results are in agreement with Wang et al. (2020), who demonstrated a strong effect of airflow velocity on the coo ling rate.

For the low velocity (0.25 m/s), the ratio between SECT and HCT is relatively constant: SECT/HCT ≈ 3. This can be explained by negligible internal resistance. In this case, $mC_p dT/dt = hS(T_{air} - T)$ and for constant air temperature $t = -\tau \ln(T^*)$ where $\tau = mC_p/(hS)$. Therefore, SECT/HCT = ln(1/8)/ln(1/2) = 3 (Defraeye et al. 2015).

For the high velocity (0.64 m/s), the CHTC (h) is higher; consequently, the Biot number ($Bi = hD/\lambda$) increases and the product's internal resistance becomes more significant (Jia et al. 2022). Therefore, SECT/HCT becomes lower than three $\left(\frac{\mathrm{SECT}}{\mathrm{HCT}}(\mathrm{R}_1) = 2.7;\ \frac{\mathrm{SECT}}{\mathrm{HCT}}(\mathrm{R}_2) = 2.8;\ \frac{\mathrm{SECT}}{\mathrm{HCT}}(\mathrm{R}_3) = 2.6\right)$.

Furthermore, the ratio of SECT obtained for the two velocities is almost the same for the three rows: $\frac{\mathrm{SECT(0.25\ m/s)}}{\mathrm{SECT\ (0.64\ m/}s)}(\mathrm{R}_1) = \frac{\mathrm{SECT(0.25\ m/}s)}{\mathrm{SECT\ (0.64\ m/}s)}(\mathrm{R}_2) = \frac{\mathrm{SECT(0.25\ m/}s)}{\mathrm{SECT\ (0.64\ m/}s)}(\mathrm{R}_3) = 1.6$. This suggests that the convective heat transfer coefficient is proportional to the square root of the air velocity since $\sqrt{\frac{0.64}{0.25}} = 1.6$. This result is in agreement with findings in the literature (Dincer 1994).

Concerning the airflow throughout the pallet, the pressure drop is mainly related to the vent holes and is, hence, proportional to the square of the velocity (kinetic energy loss through the vent holes). Therefore, the ventilation power (air flow rate multiplied by pressure drop) is roughly proportional to the air velocity cubed. Increasing velocity decreases the cooling time but to a much lesser extent. For example, Jia et al. (2022) observed that a 600% increase in air velocity (from 0.5 m/s to 3.5 m/s) is associated with a 57% decrease in SECT and a 14 334% increase in specific fan energy consumption. Therefore, from the point of view of ventilation energy, the lowest acceptable air velocity seems preferable. During storage (steady state), the airflow rate has to be sufficient to ensure a maximal acceptable product temperature $T_{max} = T_{regulatory} = 6°C$. The maximum surrounding air temperature $T_{air.max}$ is related to the respiration heat Q for one cheese item and the heat transfer coefficient h given by Equation (9).

$$Q = hS\,(T_{max} - T_{air.max}) \tag{9}$$

For a given supply air temperature $T_{air.in}$, it is then possible to estimate the airflow rate $\dot{m}_{pallet}$ (kg/s) required to offset the heat generated by the products (Equation (10)).

$$\dot{m}_{pallet}.C_{p.air}\,(T_{air.max} - T_{air.in}) \geq n_{pallet}\,Q \tag{10}$$

where n_{pallet} is the number of cheese items in a pallet

For the initial refrigeration (transient state), a maximum duration is imposed between production and storage or transport (for logistic and health reasons) for the product to reach $T_{air.max}$. The minimum air velocity required to achieve this objective is not straightforward, but the results presented can help estimate it.

3.2.2 Heat generation effect

To investigate the effect of product heat generation on the product cooling kinetics, three heat fluxes were considered (0 W, 0.05 W, 0.3 W) for the lower air velocity, 0.25 m/s (product temperature initially heterogeneous (see Section 2.3.1)).

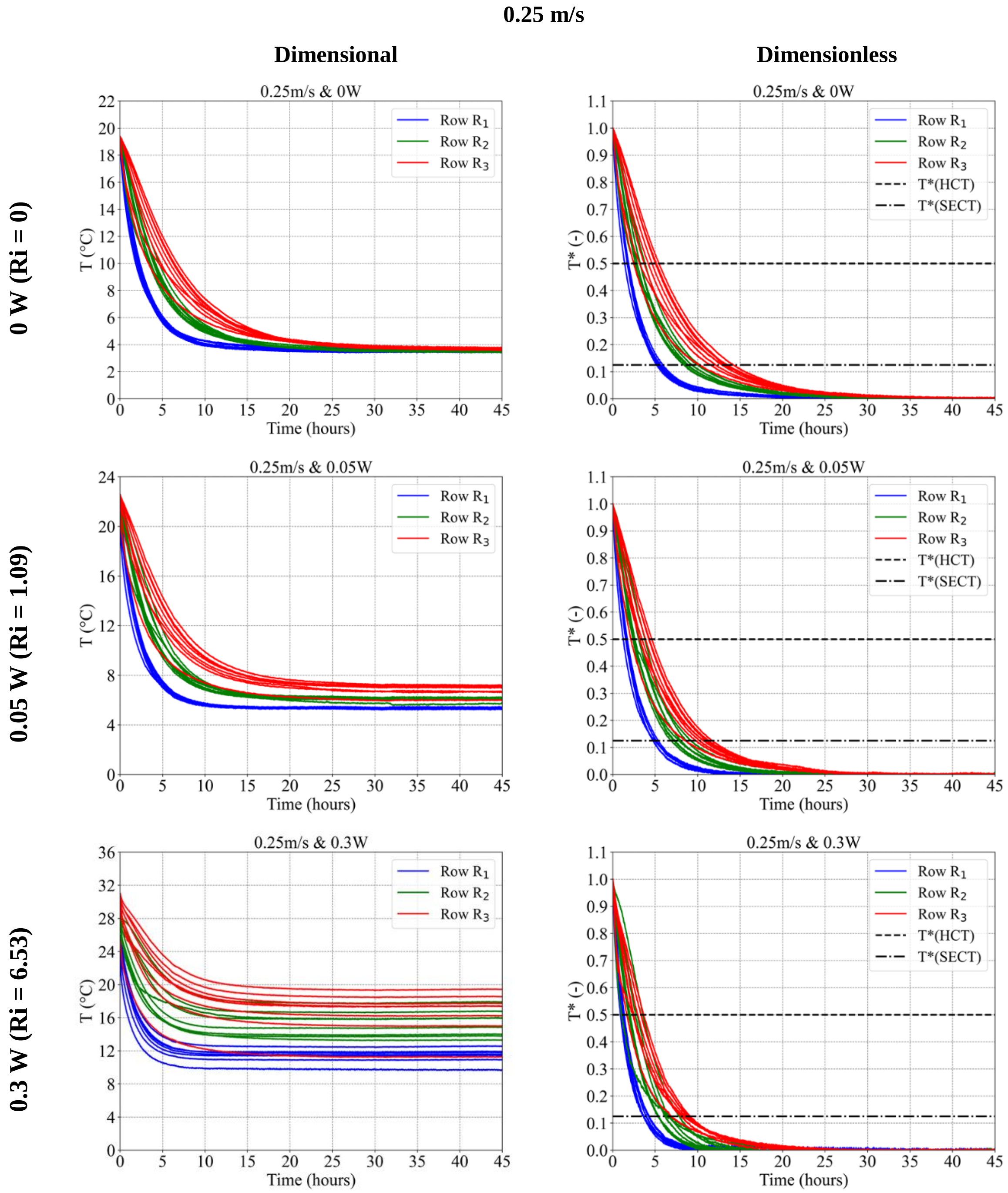

Fig. 7. Dimensional and dimensionless cooling kinetics of the plaster products within the pallet along the rows R_1, R_2 and R_3 for three heat-generated fluxes (0 W, 0.05 W and 0.3 W) and one upwind air velocity, 0.25 m/s.

Table 4: Summary of the average HCT, SECT, initial T_{in}, equilibrium T_{eq} row temperatures, and their standard deviation within the different pallet rows (R_1, R_2 and R_3) for three heat-generated fluxes (0 W, 0.05 W and 0.3 W) and one upwind air velocity, 0.25 m/s. Different letters (e.g., 'a', 'b') indicate significant differences ($p < 0.05$) based on Tukey HSD test.

Upwind air velocity $u_{air.in}$ (m/s)	**0.25**								
Heat generation flux: Q (W)	**Q = 0 (Ri = 0)**			**Q = 0.05 (Ri = 1.09)**			**Q = 0.3 (Ri = 6.53)**		
Row	**R_1**	**R_2**	**R_3**	**R_1**	**R_2**	**R_3**	**R_1**	**R_2**	**R_3**
T_{in} ± STD_{Tin} per row (°C)	**19.08** ± 0.16^{a}	**19.23** ± 0.12^{a}	**19.27** ± 0.17^{a}	**20.66** ± 0.41^{b}	**21.53** ± 0.33^{b}	**21.93** ± 0.61^{b}	**24.75** ± 0.95^{c}	**27.43** ± 0.79^{d}	**29.45** ± 1.73^{e}
T_{eq} ± STD_{Teq} per row (°C)	**3.55** ± 0.06^{a}	**3.51** ± 0.08^{a}	**3.64** ± 0.07^{a}	**5.35** ± 0.06^{b}	**6.03** ± 0.15^{b,c}	**6.83** ± 0.37^{c}	**11.31** ± 0.83^{d}	**15.32** ± 1.51^{e}	**16.62** ± 2.39^{e}
HCT ± STD_{HCT} per row (hours)	**1.71** ± 0.15^{a,f}	**3.06** ± 0.41^{b,c}	**4.21** ± 0.97^{d}	**1.59** ± 0.15^{a,f}	**2.82** ± 0.46^{c}	**3.62** ± 0.75^{c,e}	**1.19** ± 0.15^{f}	**2.23** ± 0.72^{e,a}	**2.77** ± 0.62^{c,e}
SECT ± STD_{SECT} (hours)	**5.50** ± 0.21^{a}	**9.21** ± 0.68^{b,c}	**12.58** ± 1.23^{d}	**5.03** ± 0.22^{a,f}	**7.88** ± 0.7^{c,e}	**10.53** ± 0.92^{b}	**3.86** ± 0.27^{f}	**6.23** ± 0.83^{a}	**8.38** ± 0.66^{e}

From Fig. 7, it can be seen that the equilibrium temperature of the products in the different rows is heterogeneous for Q = 0.05 W and Q = 0.3 W conditions (Pham et al. 2021). Moreover, it depends on both the positions of the products (row) and the heat generation flux (Table 4). According to Fig. 7 and Table 4, the higher the product heat generation, the higher the equilibrium temperature (see Section 3.1).

As shown in Table 4, the SECT decreases as heat generation increases. More precisely, while the difference of the SECT between the row R_3 of Q = 0 and Q = 0.05W conditions was significant ($p \leq 0.05$), the difference between the SECT for the entire pallet (all rows included) in Q = 0 and Q = 0.05W conditions was not significant ($p > 0.05$). However, the difference of the SECT for the entire pallet (all rows included) between Q = 0 and Q = 0.3W conditions was significant ($p \leq 0.05$). Between Q = 0.05 and Q = 0.3W, while results were not shown to be statistically significant ($p = 0.06 > 0.05$), it confirms the trends that the cooling is decreasing as heat generation increases. This observation is in agreement with Chourasia and Goswami (2007a). This can be explained by the dynamic interaction between two ventilation mechanisms induced by natural convection. The first mechanism, explained in Section 3.1, is related to the emergence of an ascending airflow. In fact, increasing heat generated by the products implies a higher temperature difference between air and products, which in turn means that the vertical flow of the thermal plume becomes greater and removes the heat from the products within the pallet more rapidly. The second mechanism could be explained by the emergence of a downward cold flow due to buoyancy originating from the horizontal flow when approaching the heated products. Therefore, a dynamic mixing between forced and natural convection flows involving complex heat exchange mechanisms is expected to occur. As shown in Fig. 8 and the video added to the supplementary data section, intermittent ejections or natural convection bursts have been observed in the case of high Richardson numbers (Ri = 6.53). This leads to better mixing between the cold air and the hot product. The products, therefore, reach their equilibrium temperatures at a faster rate.

Within the ventilated pallet, heat transfer occurs under transverse mixed convection regime resulting from the interaction between the main horizontal forced flow and a vertical flow induced by natural convection. The buoyancy forces in the case of transverse mixed convection promote heat exchange (Incropera et al. 2007).

In the upstream part of the pallet (row R_1), the forced convection is dominant as the velocity in the vent holes of upstream face is close to the maximal upstream velocity. However, the greatest amount of air entering by the upstream face flowed out through the lateral vent holes, implying a substantial decrease of air velocity magnitude from upstream to downstream part of the pallet. According to Pham et al. 2019b, less than 30% of the airflow rate reached the downstream part of the pallet. This decreasing of forced convection horizontal flow within the pallet gives rise to the development of a thermal plume by buoyancy forces in the downstream part of the pallet.

The effect of the thermal plume on product cooling is therefore greater downstream of the pallet than upstream, with a decrease in SECT of 1.6, 3.0 and 4.2 hours for R_1, R_2 and R_3, respectively, when increasing heat flux from 0W to 0.3W ($p \leq 0.05$, Table 4). As explained in section 3.1 and shown in Fig.5, the development of thermal plume is associated to a suction of an external cold air at lower level of the pallet inducing a more important cooling rate. The vertical flow of the thermal plume gradually warms up and evacuates the heat from products at the bottom of the pallet more quickly than those at higher levels.

In the case of forced convection, the CHTC would be independent of the heat generation and constant under the same high-velocity conditions (0.64 m/s and Ri < 0.1). Therefore, the dimensionless number: $\theta_{eq} = \frac{(T_{avg.eq} - T_{air.in})\lambda D}{Q}$ would be independent of Q. However, in the case of mixed convection (0.25 m/s; Ri ≅ 1), the CHTC is seen to be related to the heat generation flux Q. In fact, taking the average equilibrium temperature of the three rows for the low velocity (0.25 m/s), $\theta_{eq} = 1.55$ for Q = 0.05 W and $\theta_{eq} = 1.33$ for Q = 0.3 W. In addition, when heating is raised from 0.05 to 0.3 W, the SECT was divided approximately by 1.3, which is equivalent to a heating ratio 0.3/0.05 at power 0.15; in this manner, following comparison with the numerical analysis in Section **Erreur ! Source du renvoi introuvable.** (**Erreur ! Source du renvoi introuvable.**), it can be concluded that the airflow velocity exerts a greater impact than the heating rate.

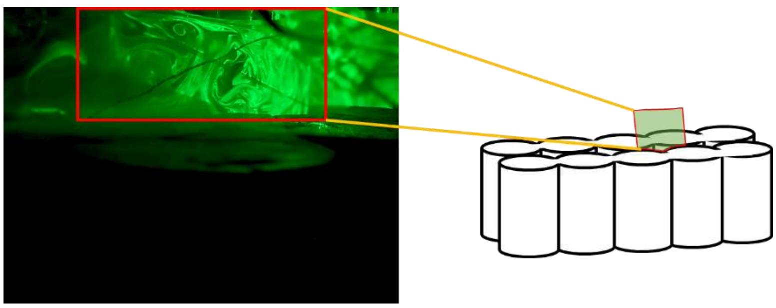

Fig. 8. Visualization of natural convection vortices in the air gap between the two BBs of box $2B_3$ at steady state for Ri = 6.53 ($u_{air.in}$ = 0.25 m/s & Q = 0.3 W). Note: The image was treated with Photopea Online Photo Editor to enhance visualization.

3.2.3 Initial temperature heterogeneity effect

In order to evaluate the effect of the heterogeneity of the initial product temperature within a pallet on the cooling kinetics, two experimental conditions: Ri = 0.17 (0.64 m/s & 0.05 W, Fig. 9) and Ri = 6.53 (0.25 m/s & 0.3 W, Fig. 10) were studied. Homogeneous and heterogeneous initial temperature conditions ($T_{in.Hom}$ and $T_{in.Het}$) were investigated in each experiment. Two repetitions of these two experiments were performed. The maximum standard deviations between the two repetitions were 0.25 h and 0.38 h for HCT and SECT.

Ri = 0.17

0.64 m/s & 0.05 W

Dimensional **Dimensionless**

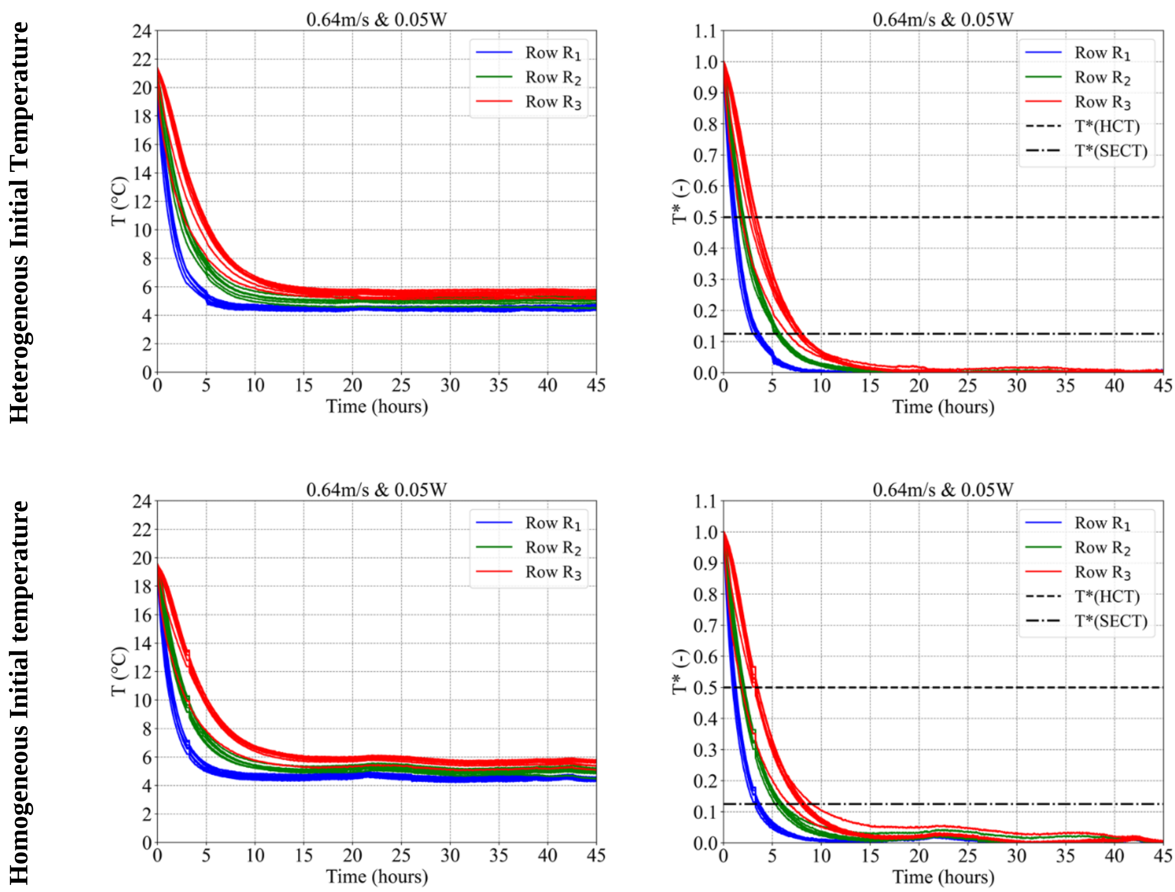

Fig. 9. Dimensional and dimensionless cooling kinetics of the different pallet rows (R_1, R_2 and R_3) for two initial temperature conditions: homogeneous ($T_{in.\ Hom}$ = 20°C) and heterogeneous for Ri = 0.17: $u_{air.in}$ = 0.64 m/s and Q = 0.3 W. For the homogeneous initial temperature experiment, an air temperature regulation issue was encountered, but thermal equilibrium was reached.

Table 5: Summary of the average HCT and SECT, initial T_{in}, equilibrium T_{eq} row temperatures, and their standard deviation within the different pallet rows (R_1, R_2 and R_3) for two initial temperature conditions: homogeneous ($T_{in.Hom}$ = 20°C) and heterogeneous for Ri = 0.17: uair.in = 0.64 m/s and Q = 0.05 W. Different letters (e.g., 'a', 'b') indicate significant differences ($p < 0.05$) based on Tukey HSD test.

Case	**Ri = 0.17 0.64 m/s & 0.05 W**					
Initial Temperature	**Heterogeneous**			**Homogeneous ≈ 20°C**		
Row	**R_1**	**R_2**	**R_3**	**R_1**	**R_2**	**R_3**
T_{in} ± STD_{Tin} per row (°C)	**19.97** ± 0.26 ^{a}	**20.62** ± 0.22 ^{b}	**21.05** ± 0.35 ^{c}	**19.05** ± 0.23 ^{d}	**19.24** ± 0.21 ^{d}	**19.35** ± 0.16 ^{d}
T_{eq} ± STD_{Teq} per row (°C)	**4.46** ± 0.11 ^{a}	**4.96** ± 0.22 ^{b}	**5.46** ± 0.23 ^{c}	**4.45** ± 0.09 ^{a}	**4.93** ± 0.20 ^{b}	**5.49** ± 0.23 ^{c}
Repetition	Repetition 1					
HCT ± STD_{HCT} per row (hours)	**1.16** ± 0.12 ^{a}	**1.92** ± 0.14^{b}	**2.97** ± 0.52 ^{c}	**1.15** ± 0.12 ^{a}	**1.97** ± 0.14 ^{b}	**3.09** ± 0.50 ^{c}
SECT ± STD_{SECT} per row (hours)	**3.48** ± 0.21 ^{a}	**5.58** ± 0.18 ^{b}	**7.64** ± 0.45 ^{c}	**3.51** ± 0.22 ^{a}	**5.79** ± 0.23 ^{b}	**8.04** ± 0.60 ^{c}
Repetition	Repetition 2					
HCT ± STD_{HCT} per row (hours)	**1.14** ± 0.12 ^{a}	**1.90** ± 0.14 ^{b}	**2.93** ± 0.50 ^{c}	**1.10** ± 0.14 ^{a}	**1.92** ± 0.13 ^{b}	**3.10** ± 0.42 ^{c}
SECT ± STD_{SECT} per row (hours)	**3.35** ± 0.20 ^{a}	**5.52** ± 0.19 ^{b}	**7.78** ± 0.45 ^{c}	**3.23** ± 0.24 ^{a}	**5.44** ± 0.26 ^{b}	**7.72** ± 0.34 ^{c}

As shown in Fig. 9, for Ri = 0.17, the temperature of the products decreases until the equilibrium temperature is reached for both conditions (homogenous and heterogeneous). According to Table 5, the initial heterogeneity of the product temperatures within the pallet exerts no significant impact as the SECT and the HCT for the two different initial conditions, homogeneous and heterogeneous, are similar ($p > 0.05$).

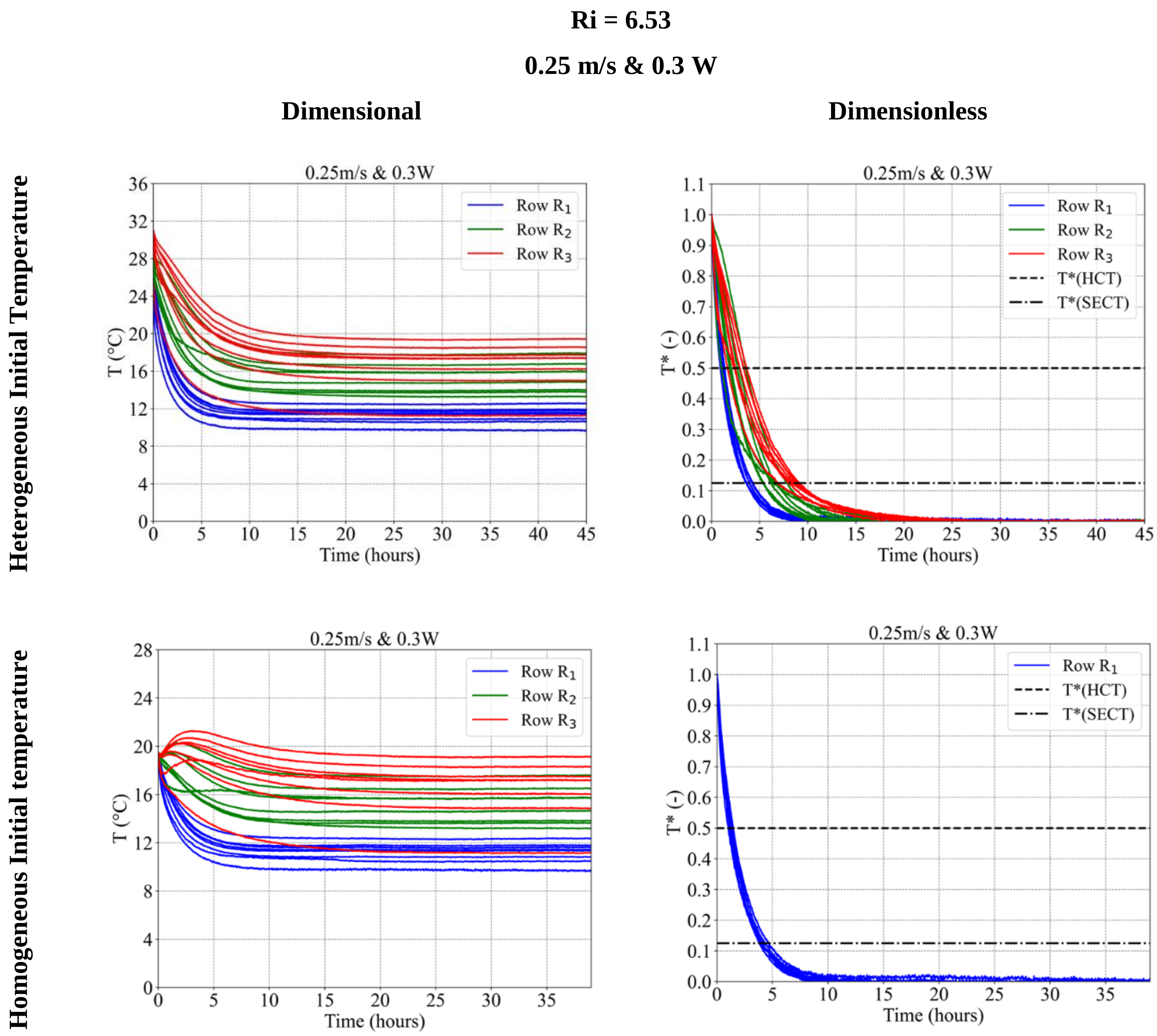

Fig. 10. Dimensional and dimensionless cooling kinetics of the different pallet rows (R_1, R_2 and R_3) for two initial temperature conditions: homogeneous ($T_{in.Hom}$ = 20°C) and heterogeneous for Ri = 6.53: $u_{air.in}$ = 0.25 m/s and Q = 0.3 W. In the case of an initial homogeneous temperature, only the dimensionless R_1 is considered.

Table 6: Summary of the average HCT and SECT, initial T_{in}, equilibrium T_{eq} row temperatures, and their standard deviation within the different pallet rows (R_1, R_2 and R_3) for two initial temperature conditions: homogeneous ($T_{in.Hom}$ = 20°C) and heterogeneous for Ri = 6.53: $u_{air.in}$ = 0.25 m/s and Q = 0.3 W. In the case of an initial homogeneous temperature, only the dimensionless R_1 is considered. Different letters (e.g., 'a', 'b') indicate significant differences ($p < 0.05$) based on Tukey HSD test.

Case	**Ri = 6.53 0.25 m/s – 0.3 W**					
Initial Temperature	**Heterogeneous**			**Homogeneous ≈ 20°C**		
Row	**R_1**	**R_2**	**R_3**	**R_1**	**R_2**	**R_3**
T_{in} ± STD_{Tin} per row (°C)	**24.75** ± 0.95 ^{a}	**27.43** ± 0.79 ^{b}	**29.45** ± 1.73 ^{c}	**19.15** ± 0.21 ^{d}	**19.32** ± 0.19 ^{d}	**19.32** ± 0.15 ^{d}
T_{eq} ± STD_{Teq} per row (°C)	**11.31** ± 0.83 ^{a}	**15.32** ± 1.51 ^{b}	**16.62** ± 2.39 ^{b}	**11.19** ± 0.79 ^{a}	**15.10** ± 1.44 ^{b}	**16.42** ± 2.33 ^{b}
Repetition	Repetition 1					
HCT ± STD_{HCT} per row (hours)	**1.19** ± 0.15 ^{a}	**2.23** ± 0.72 ^{b}	**2.77** ± 0.62 ^{b}	**1.24** ± 0.19^a	Not relevant	Not relevant
SECT ± STD_{SECT} (hours)	**3.86** ± 0.27 ^{a}	**6.23** ± 0.83 ^{b}	**8.38** ± 0.66 ^{c}	**4.08** ± 0.29 ^{a}	Not relevant	Not relevant
Repetition	Repetition 2					
HCT ± STD_{HCT} per row (hours)	**1.23** ± 0.23 ^{a}	**2.28** ± 0.47 ^{b}	**2.42** ± 0.74 ^{b}	**1.30** ± 0.17 ^{a}	Not relevant	Not relevant
SECT ± STD_{SECT} per row (hours)	**4.07** ± 0.61 ^{a}	**6.77** ± 0.75 ^{b}	**8.45** ± 0.87 ^{c}	**4.23** ± 0.37 ^{a}	Not relevant	Not relevant

For Ri = 6.53, Fig. 10 shows the temperature evolution of the products within the different rows of the pallet during the cooling process. For products in row R_1, their temperature drops gradually until the equilibrium temperature is reached for both initial temperature conditions ($T_{in.Hom}$ and $T_{in.Het}$). According to Table 6, initial temperature heterogeneity has a negligible impact on the cooling rate in row R_1 (SECT ($T_{in.Hom}$) ≈ SECT ($T_{in.Het}$)).

For the $T_{in.Hom}$ condition, as shown in Fig. 10 and Table 6, the average initial temperature of the products was 19.3 ± 0.2°C. At the start of the cooling process, a temperature increase can be observed for the products in rows R_2 and R_3. This phenomenon can be explained by the fact that at the beginning of the cooling process, the heat extracted by the convection mechanism does not offset the heat generated by the products. Indeed, for the product in row R_3, for example, the convective flux depends on the temperature of the air flowing out of box B_2, which is much higher than the $T_{air.in}$ = 4°C at the outset because it has been heated up in boxes B_1 and B_2.

Moreover, the air temperature within the pallet gradually becomes colder during the cooling process, intensifying the heat extracted by forced and natural convection, leading to a subsequent slow decrease in the product temperature until the equilibrium temperature is reached. For example, the average equilibrium temperature of the products in row R_3 is 16.4 ± 2.3°C, which is quite close to the initial temperature of 19.3 ± 0.15°C. For this reason, the HCT and the SECT in rows R_2 and R_3 were not considered.

Although the SECT and HCT of row R_1 indicate that the homogeneity of the initial temperature has no impact on the cooling rate ($p > 0.05$), the results for rows R_2 and R_3 did not make it possible to verify this conclusion. It is, therefore, interesting to go further and verify this analysis for the same Richardson number Ri = 6.53 (for the same air upwind velocity and product heat flux conditions, 0.25 m/s and 0.3 W at a homogeneous initial temperature of 30°C ($T_{in.Hom}$ = 30°C). The experimental procedure is, therefore, the same as that detailed in Section 2.3.1, with an initial set-point temperature of 30°C and an upwind air temperature remaining at 4°C.

According to Fig. 11 and Table 7, the initial temperature of the products has little impact on the cooling rate ($p \leq 0.05$), with the exception of row R_3 ($p > 0.05$), in which the cooling rate is lower when initial temperature is heterogeneous than when it is homogeneous. This position is the most influenced by natural convection, and the initial product temperature in the homogeneous case, 30°C, is lower than that in the heterogeneous case (~ 40°C).

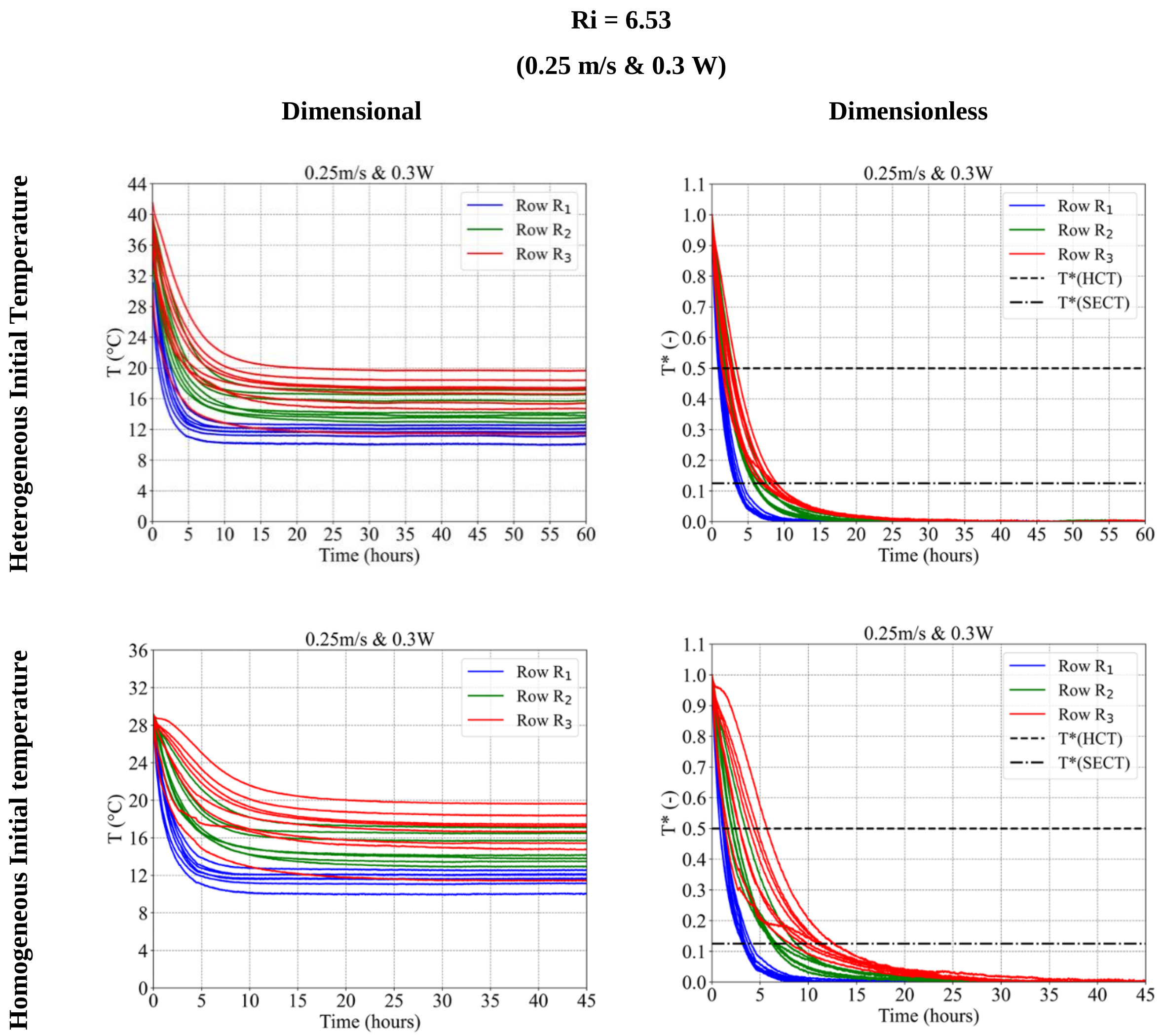

Fig. 11. Dimensional and dimensionless cooling kinetics of the different pallet rows (R_1, R_2 and R_3) for two initial temperature conditions: homogeneous ($T_{in.Hom}$ = 30 °C) and heterogeneous for Ri = 6.53: $u_{air.in}$ = 0.25 m/s = and Q = 0.3 W.

Table 7: Summary of the average HCT and SECT, initial T_{in}, equilibrium T_{eq} row temperatures, and their standard deviation within the different pallet rows (R_1, R_2 and R_3) for two initial temperature conditions: homogeneous ($T_{in.Hom}$ = 30°C) and heterogeneous for Ri = 6.53: $u_{air.in}$ = 0.25 m/s and Q = 0.3 W. Different letters (e.g., 'a', 'b') indicate significant differences ($p < 0.05$) based on Tukey HSD test.

Case	**Ri = 6.53 0.25 m/s & 0.3 W**					
Initial Temperature	**Heterogeneous**			**Homogeneous ≈ 30°C**		
Row	**R_1**	**R_2**	**R_3**	**R_1**	**R_2**	**R_3**
T_{in} ± STD_{Tin} per row (°C)	**33.80** ± 2.40 ^{a}	**37.15** ± 2.24 ^{b}	**37.32** ± 3.32 ^{b}	**28.69** ± 0.36 ^{c}	**28.8**7 ± 0.20 ^{c}	**28.71** ± 0.47 ^{c}
T_{eq} + STD_{Teq} per row (°C)	**11.65** ± 0.76 ^{a}	**14.88** ± 1.51 ^{b}	**16.39** ± 2.39 ^{b}	**11.60** ± 0.77 ^{a}	**14.83** ± 1.50 ^{b}	**16.37** ± 2.37 ^{b}
HCT ± STD_{HCT} per row (hours)	**1.20** ± 0.20 ^{a}	**2.10** ± 0.39 ^{b}	**2.36** ± 0.63 ^{b}	**1.11** ± 0.19 ^{a}	**2.31** ± 0.54 ^{b}	**3.44** ± 1.40 ^{c}
SECT ± STD_{SECT} per row (hours)	**3.60** ± 0.36 ^{a}	**6.36** ± 0.64^b	**7.98** ± 0.74 ^{c}	**3.49** ± 0.30 ^{a}	**7.01** ± 0.82 ^{b}	**10.62** ± 1.33 ^{d}

3.2.4 Interpretation of experimental results using a simple model

The parameters a = $hS/(mC_p)$ and b = $nhS/(mC_{p.air})$ were determined by minimizing the sum of the squared deviations with the experimental data: the average product temperature of rows R_1, R_2 and R_3. Fig. 12 presents the results for the two extreme Richardson number conditions ($Q \neq 0$) with a homogeneous initial product temperature ($T_{in.Hom}$ = 20 °C): Ri = 0.17 (0.64 m/s and 0.05 W) and Ri = 6.53 (0.25 m/s and 0.3 W).

Furthermore, a standard deviation band is represented for each row to consider the experimental temperature evolution heterogeneities of the different plaster products at the different pallet levels (k = 1 to 7 and k = 9) during the cooling process. The highest bandwidth related to R_3 underlines the strong variations along the height of the pallet, mainly due to the effect of the upward flow generated by natural convection.

Ri = 0.17 | **Ri = 6.53**

0.64 m/s & 0.05 W | **0.25 m/s & 0.3 W**

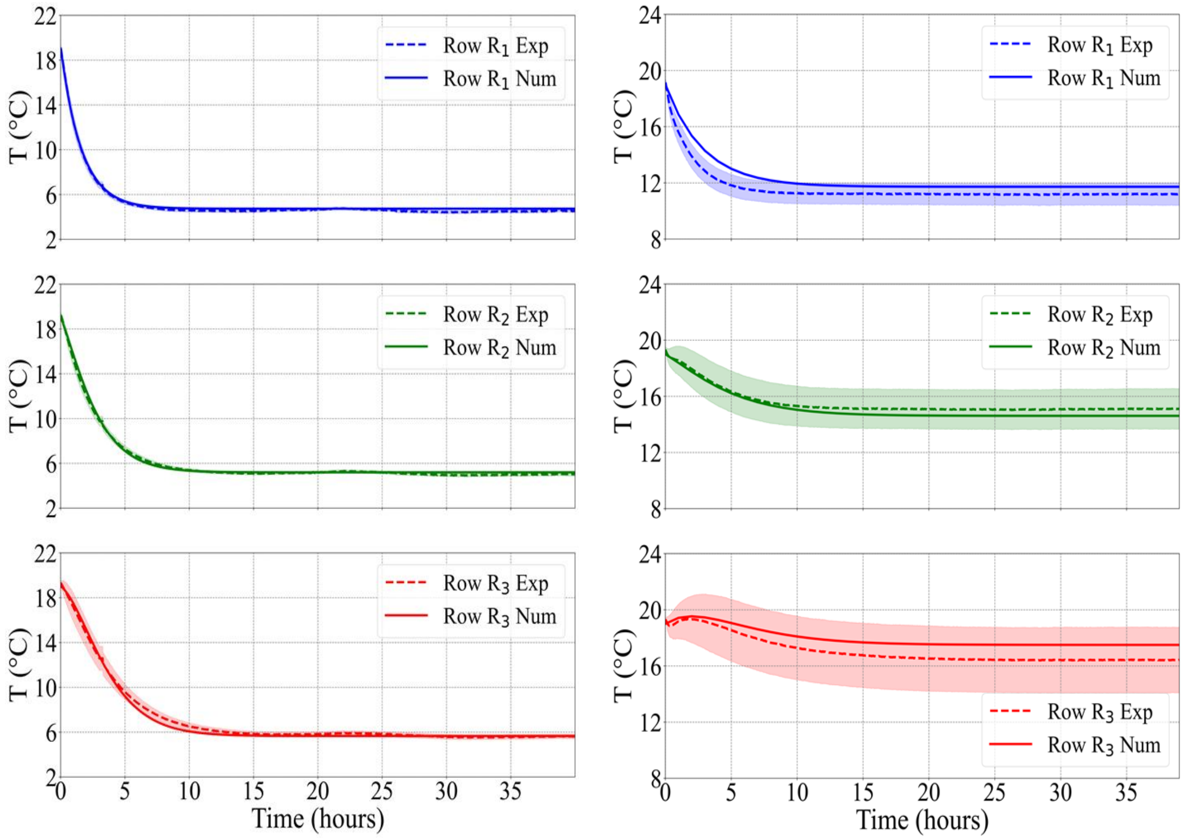

a = 0.614 ± 0.002 (h^{-1}) | a = 0.347 ± 0.001 (h^{-1})

b = 0.633 ± 0.004 | b = 0.374 ± 0.002

Fig. 12. Comparison between the numerical and experimental mean temperature evolution through the rows R_1, R_2 and R_3 for both extreme Richardson number conditions ($Q \neq 0$): Ri = 0.17 and Ri = 6.53. The STD band considers the experimental cooling kinetics heterogeneities within each pallet row. Note: The STD band for (Ri = 0.17) is thin (Max STD (R_1, R_2 and R_3) =1.31°C).

According to Fig. 12, the numerical results obtained with the simplified model show reasonable agreement with the experimental results for both investigated conditions. The model captures the increase in equilibrium temperature from R_1 to R_3 as well as the initial kinetics. In the case of Ri = 6.53 for R_3, it can even predict a slight temperature increase at the beginning of cooling.

From the estimation of parameter *a*, an average heat transfer convective coefficient h ≈ 4.9 W m^{-2} K^{-1} for $u_{air.in}$ = 0.64 m/s & Q = 0.05W (Ri = 0.17) and h ≈ 2.8 W m^{-2} K^{-1} for $u_{air.in}$ = 0.25 m/s & Q = 0.3W (Ri = 6.53) can be calculated.

As it can be seen, the predicted results remained within the range of the standard deviation bands. The differences between the predicted and experimental results can be explained by the fact that the model does not include the phenomenon of thermal plume promoted by natural convection (see Section 3.1). This probably explains the greater discrepancy between the numerical and experimental results for row R_3, where free convection is predominant. This model also assumes that the convective heat transfer coefficient is constant over the modelling domain and does not take into account the part of the airflow that exits through the side vents and the spaces between the boxes (B_1, B_2 and B_3), as mentioned by Pham et al. (2021). Since the CHTC depends on the airflow velocity (Alvarez and Flick 1999), the assumption of constant CHTC is less valid.

In addition, Moureh et al. (2022) developed a simplified model of a cheese pallet level considering the products' heat generation but without considering natural convection and the interactions between the pallet levels. All these elements highlight the importance of developing a model that takes into consideration pallet level interactions, local airflow characteristics and CHTC heterogeneities within the pallet. Besides considering the heat generation of products within the pallet, it is also essential to consider the resulting buoyancy effects induced by natural convection (thermal plume and air recirculation within the boxes).

4. Conclusion

The aim of this study, conducted under both steady-state and unsteady-state conditions, was to characterize the equilibrium temperature and cooling kinetics of heat-generating products inside a pallet under mixed convection regime. It investigates the impact of ventilation air velocity, product heat generation flux and initial product temperature heterogeneity on the cooling rate of products at different positions located in the three vertical rows of nine levels composing the pallet. A simplified model was also developed to facilitate the interpretation of experimental data.

At steady state, the results of this study confirmed the presence of a thermal plume promoted by natural convection at high Richardson number Ri > 1. For Ri = 6.53, the thermal plume is also associated with significant temperature heterogeneity in each row, particularly downstream of the pallet, with a temperature gradient of 8.2°C between bottom and top . At low Richardson numbers Ri ≤ 1, temperature within each row is more homogeneous.

At unsteady state, the results showed that an increase in air velocity from 0.25 m/s to 0.64 m/s reduces cooling times, with an average of 29% for HCT and 38% for SECT. Although heat generation increased the equilibrium temperature of the products, the products reached their equilibrium temperature at least 1.4 times faster when the heat flux per product was 0.3 W than without heat generation. This can be explained by the dynamic interaction between the main horizontal airflow and the thermal plume induced by natural convection, leading to a tranversal mixed convection which helps to remove the heat generated by the products and thus cools the products more rapidly. It can be also concluded that airflow velocity exerts a greater impact than the heating rate with a SECT divided by 1.6 when air velocity increases from 0.25 to 0.64 m/s and divided by 1.3 when heating is raised from 0.05 to 0.3W. By comparing the two initial homogeneous and heterogeneous product temperature conditions, the results showed little impact on the cooling rate except in the last row, where natural convection predominates.

The results from the simplified model showed similar trends to the experimental data, accurately capturing the initial cooling kinetics and the average equilibrium temperature within the pallet for both extreme Richardson number conditions Ri = 0.17 (0.64 m/s & 0.05 W) and Ri = 6.53 (0.25 m/s & 0.3 W). However, disparities were observed for a high Richardson number (Ri = 6.53) since the model does not consider the natural convection effect (interaction between pallet levels due to the thermal plume) and assumed uniform convective heat transfer coefficient from upstream to downstream parts of the pallet.

The simplified model presented in this study will be improved by considering the interaction between the different levels of the pallet, natural convection as well as the convective heat transfer coefficient and airflow heterogeneities from one box to another.

Data Availability

The datasets produced and analysed in this study are not publicly available for confidentiality reasons.

Competing Interests Declaration

The authors declare that they have no competing interests.

References

Aguenihanai, D., Flick, D., Duret, S., & Moureh, J. (2025). A hybrid numerical approach for characterising airflow and temperature distribution in a ventilated pallet of heat-generating products: Application to cheese. *Journal of Food Engineering*, *387*, 112323. https://doi.org/10.1016/j.jfoodeng.2024.112323

Agyeman, E. K. K., Duret, S., Flick, D., Laguerre, O., & Moureh, J. (2023). Computational Modelling of Airflow and Heat Transfer during Cooling of Stacked Tomatoes: Optimal Crate Design. *Energies*, *16*(4), 2048. https://doi.org/10.3390/en16042048

Alvarez, G., & Flick, D. (1999). Analysis of heterogeneous cooling of agricultural products inside bins: Part II: thermal study. *Journal of Food Engineering*, *39*(3), 239–245. https://doi.org/10.1016/S0260-8774(98)00166-6

Ambaw, A., Verboven, P., Delele, M. A., Defraeye, T., Tijskens, E., Schenk, A., & Nicolai, B. M. (2013). CFD Modelling of the 3D Spatial and Temporal Distribution of 1-methylcyclopropene in a Fruit Storage Container. *Food and Bioprocess Technology*, *6*(9), 2235–2250. https://doi.org/10.1007/s11947-012-0913-7

Ambaw, Mukama, M., & Opara, U. L. (2017). Analysis of the effects of package design on the rate and uniformity of cooling of stacked pomegranates: Numerical and experimental studies. *Computers and Electronics in Agriculture*, *136*, 13–24. https://doi.org/10.1016/j.compag.2017.02.015

Bejan, A. (2013). *Convection Heat Transfer*. John Wiley & Sons.

Berry, T. M., Defraeye, T., Wu, W., Sibiya, M. G., North, J., & Cronje, P. J. R. (2021). Cooling of ambient-loaded citrus in refrigerated containers: What impacts do packaging and loading temperature have? *Biosystems Engineering*, *201*, 11–22. https://doi.org/10.1016/j.biosystemseng.2020.11.002

Božiková, M., & Hlaváč, P. (2016). Thermal properties of selected cheeses samples. *Journal of Central European Agriculture*, *17*(1), 63–74. https://doi.org/10.5513/JCEA01/17.1.1672

Chourasia, M. K., & Goswami, T. K. (2006). Simulation of Transport Phenomena during Natural Convection Cooling of Bagged Potatoes in Cold Storage, Part I: Fluid Flow and Heat Transfer. *Biosystems Engineering*, *94*(1), 33–45. https://doi.org/10.1016/j.biosystemseng.2006.02.003

Chourasia, M. K., & Goswami, T. K. (2007). CFD simulation of effects of operating parameters and product on heat transfer and moisture loss in the stack of bagged potatoes. *Journal of Food Engineering*, *80*(3), 947–960. https://doi.org/10.1016/j.jfoodeng.2006.07.015

Dawood, H. K., Mohammed, H. A., Che Sidik, N. A., Munisamy, K. M., & Wahid, M. A. (2015). Forced, natural and mixed-convection heat transfer and fluid flow in annulus: A review. *International Communications in Heat and Mass Transfer*, *62*, 45–57. https://doi.org/10.1016/j.icheatmasstransfer.2015.01.006

Defraeye, T., Cronjé, P., Berry, T., Opara, U. L., East, A., Hertog, M., et al. (2015). Towards integrated performance evaluation of future packaging for fresh produce in the cold chain. *Trends in Food Science & Technology*, *44*(2), 201–225. https://doi.org/10.1016/j.tifs.2015.04.008

Defraeye, T., Lambrecht, R., Delele, M. A., Tsige, A. A., Opara, U. L., Cronjé, P., et al. (2014). Forced-convective cooling of citrus fruit: Cooling conditions and energy consumption in relation to package design. *Journal of Food Engineering*, *121*, 118–127. https://doi.org/10.1016/j.jfoodeng.2013.08.021

Delahaye, A., Gahartian, J., Jouquin, C., Oignet, J., & Ndoye, F. T. (2019). Dispositif de calorimétrie pour la mesure de flux de chaleur dégagés au cours de l'entreposage de fromages. https://hal.inrae.fr/hal-04273727. Accessed 24 November 2023

Dincer, I. (1994). Development of new effective Nusselt-Reynolds correlations for air-cooling of spherical and cylindrical products. *International Journal of Heat and Mass Transfer*, *37*(17), 2781–2787. https://doi.org/10.1016/0017-9310(94)90395-6

Han, J.-W., Zhao, C.-J., Qian, J.-P., Luis, R.-G., & Xiang, Z. (2018). Numerical modeling of forced-air cooling of palletized apple: Integral evaluation of cooling efficiency. *International Journal of Refrigeration*, 11.

Han, J.-W., Zhao, C.-J., Yang, X.-T., Qian, J.-P., & Fan, B.-L. (2015). Computational modeling of airflow and heat transfer in a vented box during cooling: Optimal package design. *Applied Thermal Engineering*, *91*, 883–893. https://doi.org/10.1016/j.applthermaleng.2015.08.060

Hélias, A., Mirade, P.-S., & Corrieu, G. (2007). Modeling of Camembert-Type Cheese Mass Loss in a Ripening Chamber: Main Biological and Physical Phenomena. *Journal of Dairy Science*, *90*(11), 5324–5333. https://doi.org/10.3168/jds.2007-0272

Hoang, H.-M., Duret, S., Flick, D., & Laguerre, O. (2015). Preliminary study of airflow and heat transfer in a cold room filled with apple pallets: Comparison between two modelling approaches and experimental results. *Applied Thermal Engineering*, *76*, 367–381. https://doi.org/10.1016/j.applthermaleng.2014.11.012

Iezzi, R., Francolino, S., & Mucchetti, G. (2011). Natural convective cooling of cheese: Predictive model and validation of heat exchange simulation. *Journal of Food Engineering*, *106*(1), 88–94. https://doi.org/10.1016/j.jfoodeng.2011.04.016

Incropera, F. P., DeWitt, D. P., Bergman, T. L., & Lavine, A. S. (Eds.). (2007). *Fundamentals of heat and mass transfer* (6. ed.). Hoboken, NJ: Wiley.

Jia, B., Yang, L., Zhang, L., Li, X., Liu, B., Chen, F., & Zhang, Q. (2022). Energy consumption in relation to the number of stacked packages in forced air pre-cooling of apples. *Journal of Food Process Engineering*, *45*(5), e14021. https://doi.org/10.1111/jfpe.14021

Joye, D. D. (2003). Pressure drop correlation for laminar, mixed convection, aiding flow heat transfer in a vertical tube. *International Journal of Heat and Fluid Flow*, *24*(2), 260–266. https://doi.org/10.1016/S0142-727X(02)00238-2

Khanafer, K., Vafai, K., & Lightstone, M. (2002). Mixed convection heat transfer in two-dimensional open-ended enclosures. *International Journal of Heat and Mass Transfer*, *45*(26), 5171–5190. https://doi.org/10.1016/S0017-9310(02)00219-3

Le Page, J.-F. L., Chevarin, C., Kondjoyan, A., Daudin, J.-D., & Mirade, P.-S. (2009). Development of an approximate empirical-CFD model estimating coupled heat and water transfers of stacked food products placed in airflow. *Journal of Food Engineering*, *92*(2), 208–216. https://doi.org/10.1016/j.jfoodeng.2008.11.001

Moureh, J., Pham, A. T., & Flick, D. (2022). Simplified model of airflow and heat transfer in a pallet of food product generating heat. *Journal of Food Process Engineering*, *45*(7). https://doi.org/10.1111/jfpe.13953

Moureh, J., Tapsoba, S., Derens, E., & Flick, D. (2009). Air velocity characteristics within vented pallets loaded in a refrigerated vehicle with and without air ducts. *International Journal of Refrigeration*, *32*(2), 220–234. https://doi.org/10.1016/j.ijrefrig.2008.06.006

O'Sullivan, J. L., Ferrua, M. J., Love, R., Verboven, P., Nicolaï, B., & East, A. (2017). Forced-air cooling of polylined horticultural produce: Optimal cooling conditions and package design. *Postharvest Biology and Technology*, *126*, 67–75. https://doi.org/10.1016/j.postharvbio.2016.11.019

Ozisik, M. N. (1985). *Heat transfer : a basic approach*. New York : McGraw-Hill. http://archive.org/details/heattransferbasi00ozis. Accessed 7 August 2024

Pham, A. T., Moureh, J., Belaidi, M., & Flick, D. (2021). CFD modelling of a pallet of heat-generating product applied to a cheese product. *International Journal of Refrigeration*, *128*, 163–176. https://doi.org/10.1016/j.ijrefrig.2021.03.011

Pham, A. T., Moureh, J., & Flick, D. (2019a). Experimental characterization of heat transfer within a pallet of product generating heat. *Journal of Food Engineering*, *247*, 115–125. https://doi.org/10.1016/j.jfoodeng.2018.12.003

Pham, A. T., Moureh, J., & Flick, D. (2019b). Experimental characterization of airflow within a pallet of product generating heat: Application for cheese product. *International Journal of Refrigeration*, *106*, 89–103. https://doi.org/10.1016/j.ijrefrig.2019.06.022

Ruuska, T., Vinha, J., & Kivioja, H. (2017). Measuring thermal conductivity and specific heat capacity values of inhomogeneous materials with a heat flow meter apparatus. *Journal of Building Engineering*, *9*, 135–141. https://doi.org/10.1016/j.jobe.2016.11.011

Sajadiye, S. M., & Zolfaghari, M. (2017). Simulation of in-line versus staggered arrays of vented pallet boxes for assessing cooling performance of orange in cool storage. *Applied Thermal Engineering*, 13. https://doi.org/10.1016/j.applthermaleng.2016.12.063

Tanner, D. J., Cleland, A. C., Opara, L. U., & Robertson, T. R. (2002). A generalised mathematical modelling methodology for design of horticultural food packages exposed to refrigerated conditions: part 1, formulation. *International Journal of Refrigeration*, *25*(1), 33–42. https://doi.org/10.1016/S0140-7007(01)00019-6

Wang, D., Lai, Y., Jia, B., Chen, R., & Hui, X. (2020). The optimal design and energy consumption analysis of forced air pre-cooling packaging system. *Applied Thermal Engineering*, *165*, 114592. https://doi.org/10.1016/j.applthermaleng.2019.114592

Wu, W., Cronjé, P., Verboven, P., & Defraeye, T. (2019). Unveiling how ventilated packaging design and cold chain scenarios affect the cooling kinetics and fruit quality for each single citrus fruit in an entire pallet. *Food Packaging and Shelf Life*, *21*, 100369. https://doi.org/10.1016/j.fpsl.2019.100369

Acknowledgements

The authors acknowledge and thank the French Dairy Interbranch Organization (CNIEL) and the National French Association of Research and Technology (ANRT) for the technical and financial support that they have provided. The authors thank the CNIEL project coordinator, Fanny Tenenhaus-Aziza, for her outstanding support.

The authors thank the research unit's technical team (Sébastien Saavedra, Alain Denis, Elyamin Dahmana, Seydina Ndoye and Yvanne Paviet-Salomon) for their technical help during the experiments—special thanks to Seydina Ndoye for taking and editing the videos and photos.

Funding Declaration

This work was funded by the French Dairy Interbranch Organization (CNIEL) and the National French Association of Research and Technology (ANRT).

Author information

Dihia AGUENIHANAI has contributed with methodology, conceptualization, conducting the experiments, data processing and analysis, development of the numerical model, writing the original version of the manuscript and its editing and revision.

Denis FLICK has contributed to the analysis of the results, conceptualization, methodology, numerical model development, manuscript review, and supervision.

Steven DURET has contributed to the analysis of the results, conceptualization, methodology, reviewing the manuscript and supervision.

Elyamin DAHMANA helped with the implementation of the experimental work.

Jean MOUREH has contributed to the analysis of the results, conceptualization, methodology, revision of the manuscript, funding acquisition and supervision.